



**HAL**  
open science

# An Iterative method for solving the inverse problem in Electrocardiography imaging: From body surface to heart potential.

Nejib Zemzemi, Hamed Bourenane, Hubert Cochet

► **To cite this version:**

Nejib Zemzemi, Hamed Bourenane, Hubert Cochet. An Iterative method for solving the inverse problem in Electrocardiography imaging: From body surface to heart potential.. IEEE Computers in Cardiology, MIT, Sep 2014, Cambridge, United States. hal-01065107

**HAL Id: hal-01065107**

**<https://inria.hal.science/hal-01065107>**

Submitted on 17 Sep 2014

**HAL** is a multi-disciplinary open access archive for the deposit and dissemination of scientific research documents, whether they are published or not. The documents may come from teaching and research institutions in France or abroad, or from public or private research centers.

L'archive ouverte pluridisciplinaire **HAL**, est destinée au dépôt et à la diffusion de documents scientifiques de niveau recherche, publiés ou non, émanant des établissements d'enseignement et de recherche français ou étrangers, des laboratoires publics ou privés.



a unit vector parallel to the local fibre direction and  $\sigma_{i,e}^1$  and  $\sigma_{i,e}^t$  are, respectively, the longitudinal and transverse conductivities of the intra- and extra-cellular media. The field of variables  $w$  is a vector containing different chemical concentrations and various gate variables. Its time derivative is given by the vector of functions  $g$ .

The precise definition of  $g$  and  $I_{ion}$  depend on the electrophysiological transmembrane ionic model. In the present work we make use of one of the biophysically detailed human ventricular myocyte model [10]. Figure 1 provides a geometrical representation of the domains considered to compute extracellular potentials in the human body. In the torso domain  $\Omega_T$ , the electrical potential  $u_T$  is described by the Laplace equation.

$$\begin{cases} \operatorname{div}(\sigma_T \nabla u_T) = 0, & \text{in } \Omega_T, \\ \sigma_T \nabla u_T \cdot \mathbf{n}_T = 0, & \text{on } \Gamma_{\text{ext}}. \end{cases} \quad (2)$$

where  $\sigma_T$  stands for the torso conductivity tensor and  $\mathbf{n}_T$  is the outward unit normal to the torso external boundary  $\Gamma_{\text{ext}}$ .

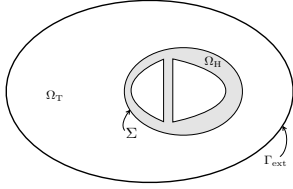


Fig. 1. Two-dimensional geometrical description: heart domain  $\Omega_H$ , torso domain  $\Omega_T$  (extramyo-cardial regions), heart-torso interface  $\Sigma$  and torso external boundary  $\Gamma_{\text{ext}}$ .

The heart-torso interface  $\Sigma$  is supposed to be a perfect conductor. Then we have a continuity of current and potential between the extra-cellular myocardial region and the torso region.

$$\begin{cases} u_e = u_T, & \text{on } \Sigma, \\ \sigma_e \nabla u_e \cdot \mathbf{n}_T = \sigma_T \nabla u_T \cdot \mathbf{n}_T, & \text{on } \Sigma. \end{cases} \quad (3)$$

### B. Anatomical model

We use a geometry that we have segmented from a CT scan of a 43 year old woman. The DICOM images were segmented using the medical imaging software Osirix. We identify three regions in the torso domain: lungs, bones, and the rest of the torso tissue. After segmentation, we use CardioViz3D<sup>1</sup>, then we used Tetgen and INRIA meshing Software MMG3D in order to get a good quality of tetrahedral mesh.

### C. Inverse problem

ECGI allows to construct the electrical potential on the heart surface  $\Sigma$  from data measured on the body surface  $\Gamma_{\text{ext}}$ . We assume that the electrical potential is governed by the diffusion equation in the torso as shown in the previous paragraph. For a given potential data  $T$  measured on the body surface  $\Gamma_{\text{ext}}$ , the goal is to find  $u_e$  on  $\Sigma$  such that the potential data in the torso domain satisfies

<sup>1</sup><https://gforge.inria.fr/projects/cardioviz3d>

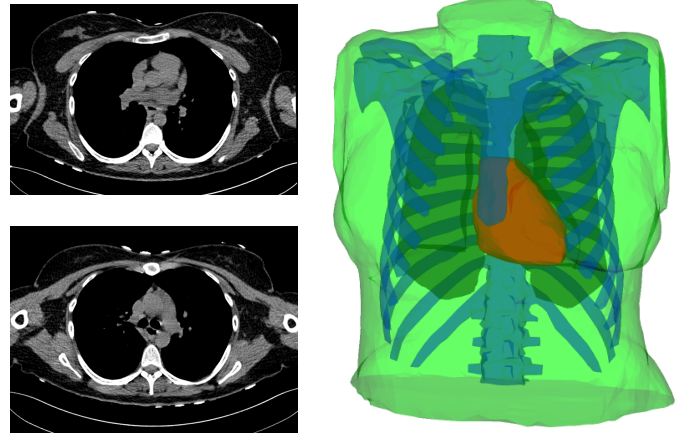


Fig. 2. Two slices of the CT-scan images (left). Torso geometry showing the epicardium (heart-torso interface  $\Sigma$ ) (red), lungs (yellow) bones (blue) and torso external boundary  $\Gamma_{\text{ext}}$  (green).

$$\begin{cases} \operatorname{div}(\sigma_T \nabla u_T) = 0, & \text{in } \Omega_T, \\ \sigma_T \nabla u_T \cdot \mathbf{n} = 0, \text{ and } u_T = T, & \text{on } \Gamma_{\text{ext}}, \\ u_T = u_e, & \text{on } \Sigma. \end{cases} \quad (4)$$

This problem is ill posed because the  $u_T$  is over determined on the boundary  $\Gamma_{\text{ext}}$ , where we have two boundary conditions to be satisfied. In order to find  $u_e$ , we use the KMF iterative method which works as a filter of the ill posedness [5], [11]. For a given electrical potential distribution on the body surface  $T$  and an initial guess about  $u^0$ , we can build two sequences  $(v^n, u^n)$  as follows

$$\begin{cases} \operatorname{div}(\sigma_T \nabla v^{n+1}) = 0, & \text{in } \Omega_T, \\ \sigma_T \nabla v^{n+1} \cdot \mathbf{n} = 0, & \text{on } \Gamma_{\text{ext}}, \\ v^{n+1} = u^n, & \text{on } \Sigma. \end{cases} \quad (5)$$

$$\begin{cases} \operatorname{div}(\sigma_T \nabla u^{n+1}) = 0, & \text{in } \Omega_T, \\ u^{n+1} = T, & \text{on } \Gamma_{\text{ext}}, \\ \sigma_T \nabla u^{n+1} \cdot \mathbf{n} = \sigma_T \nabla v^{n+1} \cdot \mathbf{n}, & \text{on } \Sigma. \end{cases} \quad (6)$$

The flux of  $v^{n+1}$ , solution of equation (5), depends linearly on  $u^n$ . We denote by  $S_N$  the Dirichlet to Neumann application that maps  $u^n|_{\Sigma}$  to  $(\sigma_T \nabla v^{n+1} \cdot \mathbf{n})|_{\Sigma}$ ,

$$(\sigma_T \nabla v^{n+1} \cdot \mathbf{n})|_{\Sigma} = S_N * u^n|_{\Sigma}.$$

On the other hand the application that maps  $v^{n+1}$  to  $u^{n+1}$  solution of equation (6) is affine and could be written as follows,

$$u^{n+1}|_{\Sigma} = S_D(\sigma_T \nabla v^{n+1} \cdot \mathbf{n})|_{\Sigma} + S_{rhs} T,$$

where  $S_D$  is the Neumann to Dirichlet operator and  $S_D(\sigma_T \nabla v^{n+1} \cdot \mathbf{n})|_{\Sigma}$  is solution of the following problem

$$\begin{cases} \operatorname{div}(\sigma_T \nabla u) = 0, & \text{in } \Omega_T, \\ u = 0, & \text{on } \Gamma_{\text{ext}}, \\ \sigma_T \nabla u \cdot \mathbf{n} = \sigma_T \nabla v^{n+1} \cdot \mathbf{n}, & \text{on } \Sigma. \end{cases} \quad (7)$$

The operator  $S_{rhs}$  maps the BSP  $T$  to the residual part  $S_{rhs}T$ , the solution of the following problem on  $\Sigma$

$$\begin{cases} \operatorname{div}(\sigma_T \nabla u) = 0, & \text{in } \Omega_T, \\ u = T, & \text{on } \Gamma_{\text{ext}}, \\ \sigma_T \nabla u \cdot \mathbf{n} = 0, & \text{on } \Sigma. \end{cases} \quad (8)$$

Note that if we consider a static geometry, operators  $S_N$ ,  $S_D$  and  $S_{rhs}$  are computed once for all, since they depend only on the mesh and the conductivities in the torso represented by  $\sigma_T$ . Computing  $S_N$ ,  $S_D$  and  $S_{rhs}$  avoids solving a 3D finite element problem at each iteration and allows a real time solving of the inverse problem.

### III. NUMERICAL RESULTS

We start by generating synthetic data using an ECG simulator based on the bidomain model. We generate BSPs for two heart cases, a healthy and a fibrillation conditions. The model parameters are the same in both cases they only differ by the stimulation protocols: In the first case, the heart is stimulated in the apex and the electrical wave propagates from apex to base. We refer to this simulation as a normal or healthy case. In the second case we apply a S1-S2 protocol, in order to produce a re-entry wave, we refer to this case as a fibrillation or re-entree case. These two cases will be considered as our gold standard data. Further informations about the forward problem modelling could be found in [6], [7]. For each time step, we extract BSPs, we add 5% of noise and we use it as the given data  $T$ . we then solve the inverse problem following the KMF method explained in the previous paragraph. In Fig.3 (respectively, Fig.4), we show snapshots of the electrical potential distribution in the body (including heart surface and torso volume), in these snapshots we compare the inverse solution to the gold standard normal (respectively, re-entree) case. The distribution of the

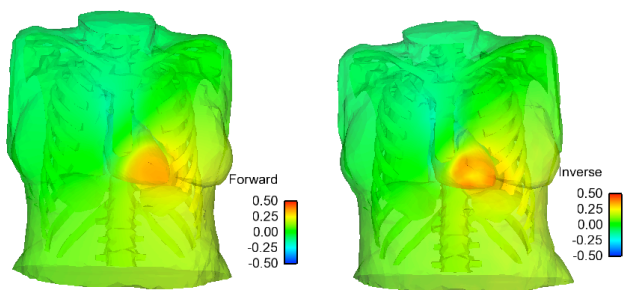


Fig. 3. Snapshots of the potential distribution in the normal case. Forward solution (left) and Inverse solution (right). The color bar scale is in mV.

reconstructed electrical potential is synchronized with the gold standard electrical potential distribution in both normal and re-entree cases. We remark that the wave front is well captured but in the inverse solution it is much more smoother than in the exact solution. As shown in previous study [8], the wave front in the normal case is much accurate than in the re-entree case. Hence we will focus our study on the re-entree case. In Fig.5 (left) (respectively right), we show a comparison between the inverse and the exact solutions

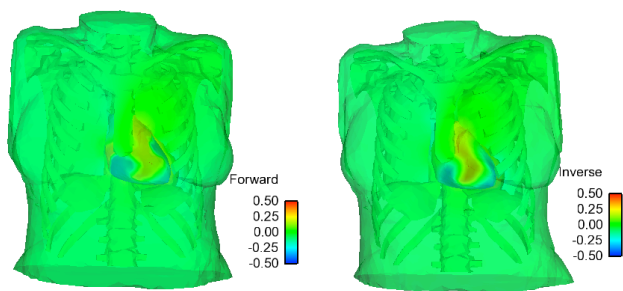


Fig. 4. Snapshots of potential distribution for re-entry case. Forward solution (left) and Inverse solution (right). The color bar scale is in mV.

of the heart potential time course at a point located in the left (respectively right) epicardium. Although signals are synchronized in both location, the magnitude of the electrical potential is clearly more accurate in the right ventricle than it is in the left one. In Fig.6 (left) (respectively, right), we

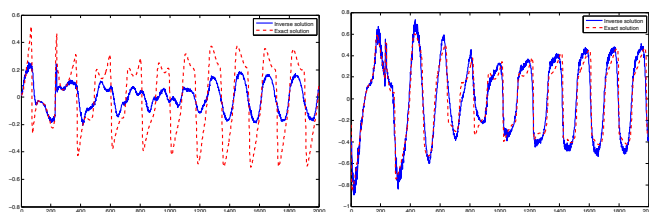


Fig. 5. Left (respectively, right): Comparison of exact (red) and inverse (blue) solutions at a given point located in the surface the left (respectively right) ventricle in the re-entree case. X-axis: time (ms) and Y-axis: potential (mV)

show the spatial distribution of the relative error in time by computing the  $l^2$  relative error in time at each point of the heart surface geometry. We see that the error is much higher in the left ventricle where its maximum reaches 75% while in the right ventricle surface it doesn't exceed 35%. In Fig

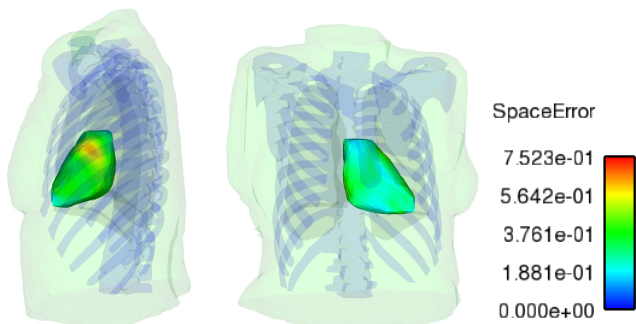


Fig. 6. Left (respectively, right): left (respectively, right) ventricle view of the heart showing the  $l^2$  relative error in time at each point of the geometry. The color bar is dimensionless.

7 (left), we show the time evolution of the space relative error by computing at each time step the spatial  $l^2$  relative error. The mean of the relative error both in space and time is 0.45. In In Fig 7 (right), we show the time evolution of the correlation coefficient (CC) which gives an idea about the spatial correlation of the inverse solution to the gold

standard data. The mean of the CC in time is 0.92. The inverse solution is 92% accurate in terms of the pattern of activation. At each point of the geometry we also compute

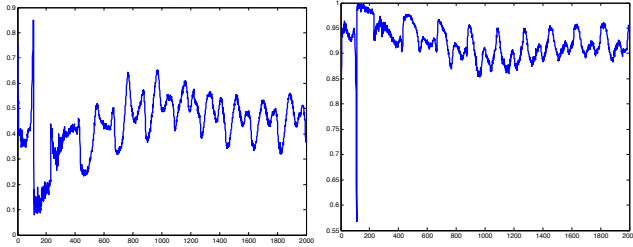


Fig. 7. Time course of the relative error (left) and correlation coefficient (right) computed using the exact and inverse solutions in case of fibrillating heart conditions. X-axis: time (ms) and Y-axis: (dimensionless).

the phase mapping of the inverse solution based on the Hilbert transform. In Fig. 8 (left) (respectively, right), we show a right ventricle view of the spatial distribution of the phase map of the gold standard solution (respectively, inverse problem solution) at time 1000 ms. We remark that the phase is correctly reconstructed which is in agreement with the results of the CC shown in Fig. 7. In Fig. 9 (left)

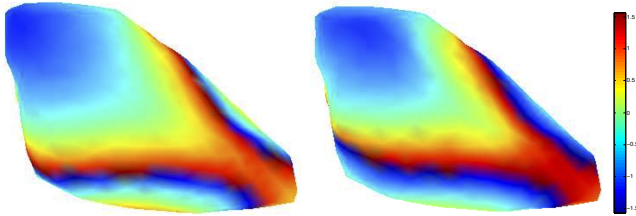


Fig. 8. Right ventricle view: Snapshots of the phase map distribution in the re-entrance case at time 1000 ms. Forward solution (left) and Inverse solution (right). The color bar scale is in Rad.

(respectively, right), we compare the exact and the inverse solutions phases at a location on the left (respectively right) ventricle. These phases correspond to the electrical potentials shown in Fig.5.

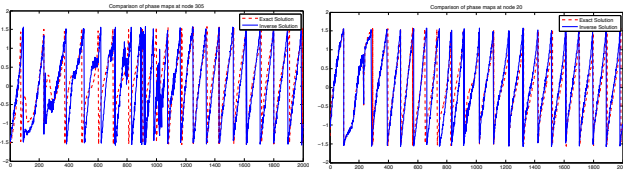


Fig. 9. Left (respectively, right): Comparison of the signal phase for exact (red) and inverse (blue) solutions at a given point located in the left (respectively right) ventricle in the re-entrance case. X-axis: time (ms) and Y-axis: potential (Rad).

#### IV. DISCUSSION

In the present work we showed an alternative to the least square approach which has been intensively used in the electrocardiography imaging community. This is the first time that the KMF algorithm is used for solving the ECGI inverse problem. We have shown that in some regions

the electrical potential is accurately computed in terms of magnitude whereas in other regions there is a high loss in the magnitude of the constructed potential mainly in the right ventricle. When the magnitude of the potential is too low the effect of noise is clearly seen on the phase map as seen in Figures 5 (left) and 9 (left) in the time window between 750 ms and 1200 ms. Even though the pattern of activation is still accurate since the mean of the CC is 0.92.

#### V. CONCLUSION

In this paper, we presented a new approach for solving the inverse problem in electrocardiography. The method is based on the Kozlov-Maz'ya-Fomin algorithm. We segmented a 3D-anatomical model of a 43 years old women torso and use it for computation. We generated synthetic gold standard data using the bidomain model for sinus rhythm and re-entree. We focused our study on the re-entree case by post processing the inverse solutions: We have compared the relative error in time and in space. We have shown the locations where the potential is not accurately reconstructed. We plotted the correlation coefficient at each time step and compared the phase maps. The assessment of the KMF method on synthetic data is a first step and regarding the results obtained in this work, we think that this method is that there is an important potential for this method to be tested in clinical applications.

#### REFERENCES

- [1] Hadamard J. Lectures on Cauchy's problem in linear partial differential equations. New Haven: Yale University Press, 1923.
- [2] Zakharov E, Kalinin A. Algorithms and numerical analysis of dc fields in a piecewise-homogeneous medium by the boundary integral equation method. *Computational Mathematics and Modeling* 2009; 20(3):247–257.
- [3] Ghosh S, Rudy Y. Application of l1-norm regularization to epicardial potential solution of the inverse electrocardiography problem. *Annals of Biomedical Engineering* 2009;37(5):902912.
- [4] Denisov A, Zakharov E, Kalinin A, Kalinin V. Numerical methods for some inverse problems of heart electrophysiology. *Differential Equations* 2009;45(7):1034–1043.
- [5] Kozlov VA, Maz'ya VG, Fomin A. An iterative method for solving the cauchy problem for elliptic equations. *Zhurnal Vychislitelnoi Matematiki i Matematicheskoi Fiziki* 1991;31(1):64–74.
- [6] Zemzemi N, Bernabeu M, Saiz J, Rodriguez B. Simulating Drug-Induced Effects on the Heart: From Ion Channel to Body Surface Electrocardiogram. *Functional Imaging and Modeling of the Heart* 2011;259–266.
- [7] Zemzemi N. Étude théorique et numérique de l'activité électrique du cœur: Applications aux électrocardiogrammes. Ph.D. thesis, Université Paris XI, 2009. <http://tel.archives-ouvertes.fr/tel-00470375/en/>.
- [8] Zemzemi N. An iterative method for solving the inverse problem in electrocardiography in normal and fibrillation conditions: A simulation study. In *International Conference of Electrocardiology (ICE)*, 2014. International Society of Electrocardiology, 2014; 53–56.
- [9] Tung L. A bi-domain model for describing ischemic myocardial D-C potentials. Ph.D. thesis, MIT, 1978.
- [10] Ten Tusscher K, Panfilov A. Cell model for efficient simulation of wave propagation in human ventricular tissue under normal and pathological conditions. *Physics in medicine and biology* 2006; 51:6141.
- [11] Lesnic D, Elliott L, Ingham D. An iterative boundary element method for solving numerically the cauchy problem for the laplace equation. *Engineering analysis with boundary elements* 1997;20(2):123–133.